Proceedings of the ASME 2010 International Design Engineering Technical Conferences & Computers and Information in Engineering Conference
IDETC/CIE 2010
August 15-18, 2010, Montreal, Quebec, Canada

DETC2010-29129

OPTIMIZING THE UNRESTRICTED PLACEMENT OF TURBINES OF DIFFERING ROTOR DIAMETERS IN A WIND FARM FOR MAXIMUM POWER GENERATION

Souma Chowdhury***
Rensselaer Polytechnic Institute
Troy, New York 12180
chowds@rpi.edu

Achille Messac*†
Rensselaer Polytechnic Institute
Troy, New York 12180
messac@rpi.edu

Jie Zhang***
Rensselaer Polytechnic Institute
Troy, New York 12180
zhangj17@rpi.edu

Luciano Castillo**
Rensselaer Polytechnic Institute
Troy, New York 12180
castil2@rpi.edu

Jose Lebron***
Rensselaer Polytechnic Institute
Troy, New York 12180
lebroj@rpi.edu

ABSTRACT

This paper presents a new method (the Unrestricted Wind Farm Layout Optimization (UWFLO)) of arranging turbines in a wind farm to achieve maximum farm efficiency. The powers generated by individual turbines in a wind farm are dependent on each other, due to velocity deficits created by the wake effect. A standard analytical wake model has been used to account for the mutual influences of the turbines in a wind farm. A variable induction factor, dependent on the approaching wind velocity, estimates the velocity deficit across each turbine. Optimization is performed using a constrained Particle Swarm Optimization (PSO) algorithm. The model is validated against experimental data from a wind tunnel experiment on a scaled down wind farm. Reasonable agreement between the model and experimental results is obtained. A preliminary wind farm cost analysis is also performed to explore the effect of using turbines with different rotor diameters on the total power generation. The use of differing rotor diameters is observed to play an important role in improving the overall efficiency of a wind farm.

KEYWORDS

Optimization, Particle Swarm, Wake Model, Wind Energy

INTRODUCTION

In recent years, growing concerns about climate change and unpredictable fossil fuel prices have increased the focus on sustainable energy resources, such as wind and solar energy. The horizontal axis wind turbine is the most popular form of wind turbine, which has been in existence since the 13th century [1]. Nevertheless, the practical viability of energy production (governed by such factors as need for "large scale energy production" and "return on investment") has been restraining the exploitation of the full potential of wind energy. The 2008 worldwide nameplate capacity of wind powered generators is 121 GW, which is only approximately 1.5% of worldwide electricity consumption [2]. This calls for improvement in wind power generation technology, which can be realized in part through optimization of individual wind turbines, as well as of entire wind farms.

Wind Farm Optimization (WFO)

† Address all correspondence to this author
* Professor, Department of Mechanical Aerospace and Nuclear Engineering
** Associate Professor, Department of Mechanical Aerospace and Nuclear Engineering
*** Doctoral Student, Department of Mechanical Aerospace and Nuclear Engineering

Copyright © 2010 by ASME

Significant work has been done in the design optimization of single wind turbines. Wind turbines that can operate at acceptable levels of efficiency are commercially available. Wind energy sources generally appear in the form of wind farms that consist of multiple wind turbines located in a particular arrangement over a substantial stretch of land (onshore), or water body (offshore). It has been shown by Sorensen et al. [3] that the total power extracted by a wind farm is significantly less than the simple product of the power extracted by a standalone turbine and the number (N) of identical turbines in the farm. Comparison of (i) the product of the power curve of a standalone turbine and N, and (ii) the power curve of the whole wind farm (Park Power Curve (PPC)) reveals the same. The discrepancy can be as high as 12.4% of the former (farm efficiency), as shown by Sorensen et al. [3] in the case of an offshore wind farm in Denmark.

This deficiency can be attributed to the loss in the availability of energy due to wake effects – i.e. the shading effect [4] of a wind turbine on other wind turbines downstream from it. The net energy loss due to this mutual shading depends mainly on the geometric arrangement of wind turbines in a farm. Moreover, the possible economic profit from a wind farm is one of the guiding factors in planning a wind energy project, which in turn depends on the farm efficiency and the number of turbines to be installed. Hence an optimal layout of turbines that ensures maximum farm efficiency is of utmost importance in conceiving a wind farm project.

Some notable work has been done in layout optimization of wind farms. The Offshore Wind Farm Layout Optimization (OWFLO) project [5] endeavors to minimize the Cost of Energy (COE) of the wind farm using the software OWFLO. OWFLO uses the PARK wake model by Katic et al. [6], but also has the flexibility to use other wake models. Both gradient based and heuristic algorithms have been used for optimization purposes. As a part of the Danish PSO project, Sorensen et al. [3] used the software WindPRO for wind farm layout analysis. WindPRO employs different wake models, such as by Jensen et al. [7], EWTS II and eddy viscosity model [8]. The Riso Farm model was used by Beyer et al. [4] in conjunction with genetic algorithms to optimize the wind farm layout for maximum economic profit. A similar approach utilizing genetic algorithms has also been made by Mosetti et al. [9], Grady et al. [10] and Sisbot et al. [11].

Energy deficit due to mutual shading effects is predicted using wake models that give a measure of both the growth of the wake and the velocity deficit in the wake with distance behind the wind turbine. The Park wake model originally developed by N. O. Jenson [7] and Katic et al. [6], has been one of the most popular analytical wake models used in wind farm modeling. The modified Park wake model and the eddy viscosity wake model are other standard wake models.

Limitations of Existing WFO Models

Existing wind farm models generally assume either an array like (row-column) farm layout, or divide the wind farm into a discrete grid in order to search for the optimum grid locations of a fixed number of wind turbines. Such restrictions on locating turbines in a wind farm can introduce an appreciable source of sub-optimality. In the UWFLO model developed in this project, these assumptions have been avoided. The "grid-wise location" scheme does tend towards a fully unrestricted turbine locating scheme, if the grid size is sufficiently small (of the order of rotor diameters). However, that approach may require excessive computational resources (higher number of function evaluations for optimization) in order to converge. Most of the popular wind farm models adopt a constant value of the induction factor to account for the energy drop in the wind, while flowing across a turbine. In reality, the induction factor for any given turbine design generally depends on the tip speed ratio of the turbine and on the velocity of the incoming wind. Hence, in the present study, a variable induction factor that depends on the incoming wind velocity (for a given tip speed ratio) has been employed.

In addition to the above stated limitations, existing approaches confine the layout optimization study to wind farms comprised of identical wind turbines. However, in planning a wind farm, an appropriate combination of turbines with different dimensions might prove to be economically more beneficial. The UWFLO model, in conjunction with a standard wind farm cost analysis model, explores the benefits of using turbines with different rotor diameters.

Available analytical models, including UWFLO, make far reaching assumptions and approximations, especially in modeling the wake velocity deficit. These can lead to results that fall short of the actual real life wind farm scenario. A Computational Fluid Dynamics (CFD) model is likely to achieve a more accurate estimation of the wake velocities and the power extracted by the turbines. However, a high fidelity CFD simulation of the wind flowing across an entire wind farm would involve substantial computational complexity and process runtime. Also, in recent CFD analyses, turbine rotors have been modeled as a static permeable disc, which does not capture wake rotation and corresponding energy loss effects.

Development of the UWFLO Model

In the UWFLO model, the growth of the wake and the energy deficit behind a turbine are calculated using the wake growth model proposed by Frandsen et al. [12] and the velocity deficit model presented by Katic et al. [6], respectively. However, these studies assume a uniform array layout for the wind farm. In the current work, this restrictive assumption is not made; hence the effect of the merging of wakes (wake superposition) from different turbines upwind of any particular wind turbine has been accounted for using the basic principles of energy conservation. Also, the possibility of

Copyright © 2010 by ASME

a turbine being 'partially' in the wake of another turbine (upwind) has been taken into account, which is often lacking in wind farm power generation models. The wind farm model developed in UWFLO is first validated against experimental data obtained from Cal et al. [13]. In this wind tunnel experiment, the velocity distributions within a 3x3 array of model wind turbines are analyzed using a stereo PIV system. The power generated by the last row center turbine has also been estimated for different incoming wind velocities.

In the present work, layout optimization is performed on a wind farm similar to that in the experimental setup [13] in terms of the farm dimensions and the total number of turbines involved (nine). The net power generated by the wind farm is calculated as the sum of the power generated by individual wind turbines. The farm dimensions and the minimum distance required between any two turbines are treated as system constraints. A Particle Swarm Optimization (PSO) algorithm [14] is applied to optimize the farm layout with the objective of maximizing the total power generation. A robust constraint handling technique introduced by Deb et al. [15], and later adopted by Chowdhury et al. [16], is employed to deal with the inequality constraints involved in the optimization problem.

This study finds that the design domain of the wind farm power generation model has multiple local optima. PSO, being a stochastic search algorithm, deals with multimodal problems such as this significantly better than gradient based algorithms. Moreover, PSO is easy to implement and involves fewer user defined parameters that need to be adjusted when compared to some of the standard evolutionary optimization algorithms. A simple quadratic cost model has been added as a constraint in order to illustrate the effect of having turbines with different rotor diameters on the optimal farm layout.

The following are discussed in the subsequent sections.

1. Formulation of the UWFLO wind farm model (power generation model and cost model)
2. The validating wind tunnel experiment
3. A brief description of the PSO algorithm
4. Different wind farm scenarios studied and the corresponding results obtained.

UWFLO POWER GENERATION MODEL

The power generated by a wind farm is a complex function of the configuration and location of the individual wind turbines. The flow pattern inside a wind farm is also complex. Consequently, the velocity of the wind approaching each turbine and the corresponding power generated have to be estimated separately for each turbine. The former is closely dependent on the influence of turbines upwind of the turbine being analyzed. A wind farm of given dimensions, consisting of N turbines, is considered here. This wind farm is exposed to a wind profile given by [13]

$$U_\infty = b_1 \left(\frac{z}{b_2} \right)^{0.15} \tag{1}$$

where z is the vertical distance from the ground, and b_1 and b_2 are constants dependent on the terrain, surface roughness and the atmospheric conditions. However, the wake model used assumes a uniform flow equivalent to the incoming velocity integrated and averaged over the rotor area (U_0). The total power generated by the wind farm is calculated by observing the following sequence of five steps.

- **Step 1:** Each turbine is assigned a coordinate (X, Y) based on a fixed coordinate system (X_i, Y_i). This system is then transformed into another coordinate system (x, y), such that the positive x-direction is aligned with the direction of the wind (constant or variable) as expressed by

$$\begin{bmatrix} x_i \\ y_i \end{bmatrix} = \begin{bmatrix} \cos\theta & -\sin\theta \\ \sin\theta & \cos\theta \end{bmatrix} \begin{bmatrix} X_i \\ Y_i \end{bmatrix} \tag{2}$$

  Here, θ is the angle made by the direction of wind with the positive X-axis when measured in the counterclockwise direction. The distance between any two turbines (i and j) is denoted by,

$$\Delta x_{ij} = x_i - x_j, \; \Delta y_{ij} = y_i - y_j \tag{3}$$

- **Step 2:** In order to identify whether a turbine is within the influence of the wake of another turbine, an influence matrix M is created such that,

$$M_{ij} = \begin{cases} +1 & \text{if Turbine-}i\text{ influences Turbine-}j \\ -1 & \text{if Turbine-}j\text{ influences Turbine-}i \\ 0 & \text{if there is no mutual influence} \end{cases} \tag{4}$$

  where Turbine-j is in the influence of the wake created by Turbine-i if and only if,

$$\Delta x_{ij} < 0 \quad \& \quad \left| \Delta y_{ij} \right| - \frac{D_j}{2} < \frac{D_{wake,ij}}{2} \tag{5}$$

  where D_j is the rotor diameter of Turbine-j and $D_{wake,ij}$ is the diameter of the wake front due to Turbine-i approaching Turbine-j.
- **Step 3:** The turbines are ranked ($R_i = 1, 2, \ldots, N$) in the increasing order of their x-value. Thereby, the closer the turbine is to the direct wind (wind entering the farm) the lower its rank. If any two turbines have the same x-coordinate, they will be assigned the same rank.
- **Step 4:** The power generated by each turbine (say Turbine-j) is calculated sequentially in the order of its rank, i.e. starting with rank one. This method ensures that the influence of the wakes (both individual and merged)

Copyright © 2010 by ASME

from the turbines upwind can be appropriately accounted for. Turbine-*j* might be partially or completely in the wake of other turbines. The wake of each preceding turbine *k* for which $M_{kj} = 1$, is mapped onto Turbine-*j* as follows:

If the rotor of Turbine-*j* is completely in the wake of Turbine-*k*, then

$$\begin{aligned} A_{kj} &= A_j \\ A_j &= \pi D_j^{\,2}/4 \end{aligned} \tag{6}$$

and if the rotor of Turbine-*j* is partially in the wake of Turbine-*k*, then

$$A_{kj} = r_k^{\,2}\cos^{-1}\left(\frac{d^2+r_k^{\,2}-r_j^{\,2}}{2dr_k}\right)+r_j^{\,2}\cos^{-1}\left(\frac{d^2+r_j^{\,2}-r_k^{\,2}}{2dr_j}\right) -\frac{1}{2}\sqrt{\left(-d+r_k+r_j\right)\left(d-r_k+r_j\right)\left(d+r_k-r_j\right)\left(d+r_k+r_j\right)} \tag{7}$$

where r_k and r_j are the radii, A_{kj}, and d are the enclosed area and the distance between centers as shown in Fig. 1.

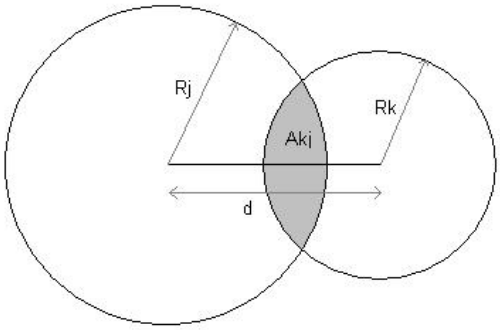

Figure 1. INTERSECTION OF A WAKE FRONT AND A TURBINE ROTOR

The contribution of the wake of each upwind Turbine-*k* (P_{kj}) towards the net kinetic energy approaching Turbine-*j* per unit time is estimated as

$$P_{kj} = \frac{A_{kj}}{A_j}U_{kj}^{\,2} \tag{8}$$

If any portion of the rotor is exposed to the direct wind (wind entering the farm), its relative contribution is calculated as

$$P_{\infty j} = \frac{A_{\infty j}}{A_j}U_{0j}^{\,2} \tag{9}$$

where $A_{\infty j}$ is the area of the rotor outside the influence of any wakes and U_{0j} is the freestream velocity averaged over the rotor diameter (for Turbine-*j*). The total wind power available to Turbine-*j* ($P_{av,j}$) is calculated as the algebraic mean of the contributions of the approaching wakes and the direct wind as relevant for each turbine. The effective wind velocity (assuming uniform flow) upstream of Turbine-*j* is calculated by Eq. (10).

$$U_k = \sqrt{\frac{2P_{av,j}}{\rho A_j}} \tag{10}$$

The power generated by this turbine (P_j) is then estimated using the formula

$$P_j = k_g k_b C_p{}'\left(\frac{1}{2}\rho\pi\frac{D_j^{\,2}}{4}U_j^{\,3}\right) \tag{11}$$

where ρ is the density of the wind. The parameters k_g and k_b are the generator efficiency (electrical efficiency) and the gearbox efficiency (mechanical efficiency), respectively. $C_p{}'$ is the coefficient of power, which is a measure of the ratio of power extracted from the wind and the power available. It is characteristic of the design of the turbine rotor and is dependent on the tip speed ratio and the incoming wind velocity. The maximum achievable value of $C_p{}'$ is 0.59 as given by the Betz limit [17]. In the remainder of the paper, the product of the efficiencies and $C_p{}'$ will be referred to as the power coefficient C_p that is

$$C_p = k_g k_b C_p{}' \tag{12}$$

- **Step 5:** The power generated by the farm, P_{farm}, is calculated as an algebraic sum of the powers generated by the individual turbines as given by

$$P_{farm} = \sum_{j=1}^{N} P_j \tag{13}$$

Wake Model

The wake model used in UWFLO, which calculates the growth of individual wakes and the velocity deficit in them has been adopted from Frandsen et al. [12]. This model employs the control volume concept that relates the thrust and power coefficients to the velocity deficit, as introduced by Lanchester [18] and Betz [17]. The growth of the wake front behind any Turbine-*j* is given by the equation

Copyright © 2010 by ASME

$$D_{wake,j} = (1 + 2\alpha s) D_j$$
$$s = \frac{x}{D_j} \tag{14}$$

where $D_{wake,j}$ is the diameter of the expanding wake front at a distance x behind Turbine-j. The parameter α is the wake spreading constant which is calculated using the formula proposed by Frandsen [19],

$$\alpha = \frac{0.5}{\ln\left(\frac{z_H}{z_0}\right)} \tag{15}$$

where z_H and z_0 are the average hub height of the turbines and the average surface roughness of the wind farm region, respectively. The velocity deficit in the wake is given by

$$U = \left(1 - \frac{2a}{(1 + 2\alpha s)^2}\right) U_j \tag{16}$$

Here, a is the induction factor, which can be calculated from the coefficient of thrust (C_t). The latter is one of the design characteristics of a turbine rotor. Equation (16) is the same as that suggested in the Park wake model described by Katic et al. [6] and Jensen [7].

UWFLO COST MODEL

Different techniques have been developed to estimate the cost (installation, operation and maintenance) of both onshore and offshore wind farms in the last twenty years, such as the Short Cut model [20], cost analysis model for the Greek market [21], OWECOP-Prob cost model [22], JEDI-wind cost model [23] and the Opti-OWECS cost model [24]. Only the first two models among these present analytical expressions of the cost as a function of different contributing factors. In addition, they do not explicitly consider the effect of the rotor diameter of the wind turbines, which can be an important factor in cost analysis. Instead, only the rated power of the wind turbines is considered, which does not account for the effect of turbine dimensions on the nature of the flow inside the wind farm. The actual power generated by the wind farm, and hence the return on investment, depends on the latter substantially.

In this study, a quadratic response surface has been developed to represent the cost of a wind farm. A m-variable quadratic response surface is expressed as

$$Cost = c_0 + \sum_{i=1}^{m} c_i v_i + \sum_{i=1}^{m} c_{ii} v_i^2 + \sum_{i=1}^{m} \sum_{\substack{j=1 \\ j \neq i}}^{m} c_{ij} v_i v_j \tag{17}$$

Where the v_i's are the variable parameters and the c_i's are the unknown coefficients. These coefficients are determined by the least squares approach, using available data. In this paper, only a single variable quadratic function is used. Equation (18) expresses the cost of a wind farm as a function of the rotor diameter of the constituent wind turbines. This function was estimated using data for wind farms in the state of New York, provided by the Wind and Hydropower Technologies program (US Department of Energy) [23].

$$Cost = 143.85 - 0.32447D - 1.4841 \times 10^{-3} D^2 \tag{18}$$

In Eq. (18), D is the diameter of the wind turbines in the farm. The above function was estimated with a relative error of 0.2 %. Sufficient data, relevant to cost analysis, is not available for wind farms with non-identical wind turbines. Hence the cost of a wind farm with non-identical wind turbines is approximated by the following equation.

$$Cost = \frac{1}{N} \sum_{i=1}^{N} Cost(D_i) \tag{19}$$

$Cost$ (D_i), specified in Eq. (19), is calculated using the formula given in Eq. (18). Though the cost of the wind farm (in a particular region) is a complex function of several factors, such as the number of turbines, labor cost and other economic factors, a simple rotor diameter based cost model has been presented here merely to explore the potential benefits of using non-identical turbines in a wind farm.

POWER GENERATION MODEL VALIDATION

Wind Tunnel Experiment [13]

Experimental measurements are used to validate the power generation model in UWFLO. The experiment consists of a scaled down wind farm that is placed in a wind tunnel as shown in Fig. 2. A 3x3 array of model wind turbines was subjected to inflow conditions that represent those of a neutrally stable boundary layer flow. Hot-wire anemometry was used to characterize the inflow properties. Measurements of the flow inside the array were performed using Stereo-Particle Image Velocimetry in 18 planes surrounding the center wind turbine of the third row, downstream. In the remainder of the paper this wind turbine will be referred to as the Turbine-8. Detailed information regarding the experiment may be found in Cal et al. [13].

The attributes of the wind farm and the incoming wind characteristics are given in Tables 1 and 2, respectively. The variation of the power coefficient (C_p) with streamwise velocity was calculated from direct torque measurements performed on Turbine-8. Extensive details of these

Copyright © 2010 by ASME

measurements can be found in Kang et al. [25]. The C_p curve presented in Fig. 3a corresponds to a constant tip speed ratio (λ) of 4.9, the one used during the experiments. Three operational points were measured and a quadratic curve fit was used to obtain a continuous function.

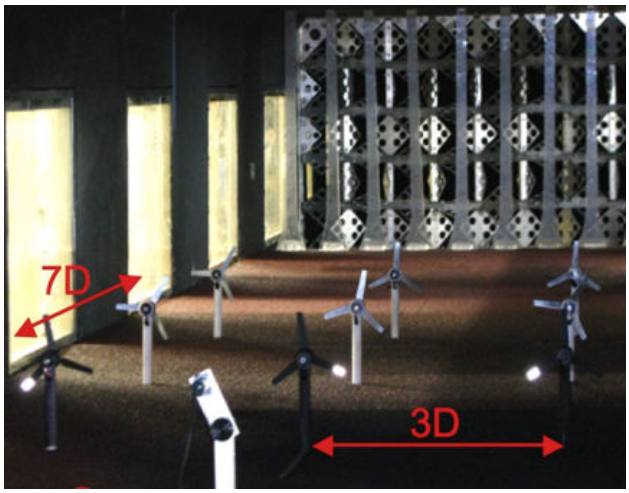

Figure 2. PHOTOGRAPH OF THE EXPERIMENTAL SETUP FROM A DOWNSTREAM LOCATION LOOKING UPSTREAM

Table 1. WIND FARM ATTRIBUTES

Attribute	**Value**
Length	1.68 m
Breadth	0.72 m
Turbine Hub Height (H)	0.12 m
Turbine Rotor Diameter (D)	0.12 m
Downwind Separation	7D
Crosswind Separation	3D
Average Surface Roughness	0.001m

Table 2. WIND CHARACTERISTICS

Parameter	**Value**
Rotor Averaged Wind Speed	7.09 m/s
Mean Velocity profile	$u(y) = 8.4(y/0.37)^{0.15}$ m/s
Wind Direction	0° with positive X-axis
Density of Air	1.2 kg/m^3

The induction factor for a wind turbine is defined by

$$a = 0.5\left(1 - \frac{U_{back}}{U_{front}}\right) \tag{20}$$

where U_{front} and U_{back} are the velocities of the wind in front of and behind the turbine, respectively. According to the ideal flow assumption, the induction factor and the coefficient of power are related by

$$C_p = 4a(1-a)^2 \tag{21}$$

Equation (21) is solved to yield the values of the induction factor, which is shown in Fig. 3b. The resulting induction factor curve is shown in Fig. 3(b). However because of insufficient data over a wider range of velocities and specific information regarding the nature of the variation of the induction factor of the experimental wind turbines, the a curve was approximated using a slope equivalent linear extrapolation beyond the point A (dashed line in Fig. 3b), instead of extrapolating the quadratic fit. This approximation was necessary because some of the wind turbines (both during validation of the model and optimization) operate in the velocity range of 5.2 to 7.1 m/s. Also, in the case of the experimental conditions, the induction factor calculated from Eq. (21) is $a \sim 0.05$, while that directly measured from the flow field is $a = 0.087$. This underestimation can be attributed to the ideal flow assumption, in which (i) rotor inefficiencies, (ii) wake of the tower and (iii) existence of the hub are neglected. Detailed information regarding the calculation of the induction factor from the velocity field may be found in Lebron et al. [26]. It is seen from Fig. 3 that the maximum values of C_p and a, which are 0.3125 and 0.095, respectively, occur at a velocity of 5.00 m/s.

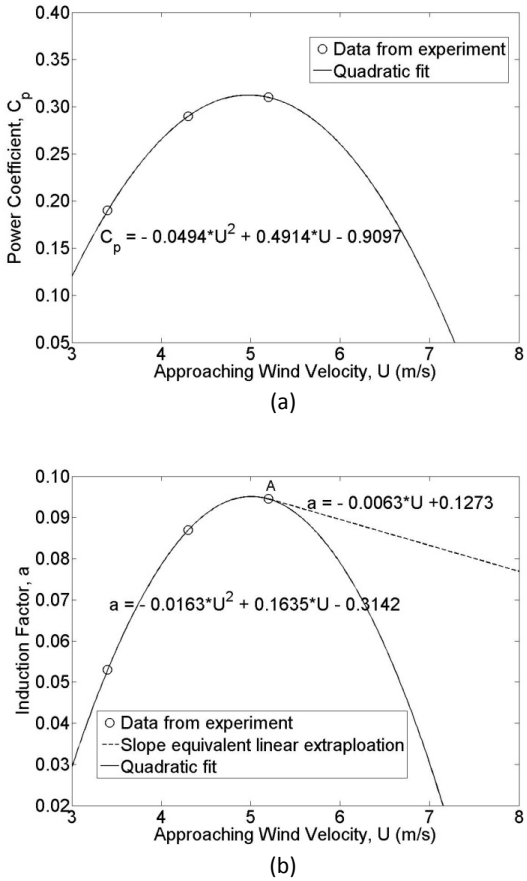

Figure 3. WIND TURBINE PERFORMANCE CURVES: (a) MEASURED POWER COEFFICIENT, (b) CALCULATED INDUCTION FACTOR FROM KANG ET AL. [21]

Copyright © 2010 by ASME

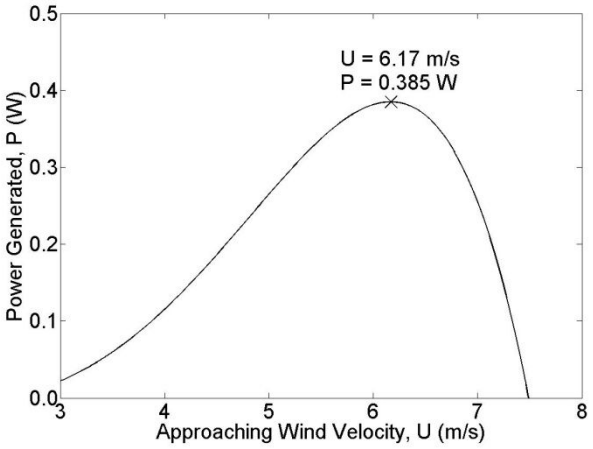

Figure 4. WIND TURBINE POWER CURVE

Figure 4 shows the variation of the actual power generated by a wind turbine as a function of the incoming wind velocity. The available wind energy increases with velocity, whereas the extent to which it can be extracted by the turbine (represented by C_p) follows a different trend as observed from Fig. 3a. Hence the power curve (Fig. 4) is a more lucid representation of the actual performance of wind turbines. It is seen that the maximum power (P = 0.385W) is generated when the approaching wind velocity is 6.17 m/s.

Model Validation Results

The power generation model is simulated using the C++ programming language. It is assumed that the wind farm is exposed to a unidirectional wind (blowing in the positive X direction), just as in the case of the experimental setup [13]. The configuration of the wind farm simulated in the model is a near replica of the wind farm experiment, and the input data used is derived from Tables 1 and 2. One difference between the UWFLO model and the experiments is that the inflow conditions in the model represent a uniform flow without turbulence. Therefore, the rotor-averaged inflow velocity of 7.09 m/s was used.

The coefficient of power, C_p, and the induction factor, a, are calculated using Eq. (20) and Eq. (21), respectively. $C_{p,max}$ is calculated to be 0.3125. The arrangement of turbines in the experiment is shown in Fig. 5. The dashed line rectangle represents the boundary of the wind farm and the numbered squares represent the corresponding turbine locations. The velocity of the wind approaching each turbine, and the corresponding power available and the power generated in the case of each turbine are shown in Figures 6, 7a and 7b, respectively.

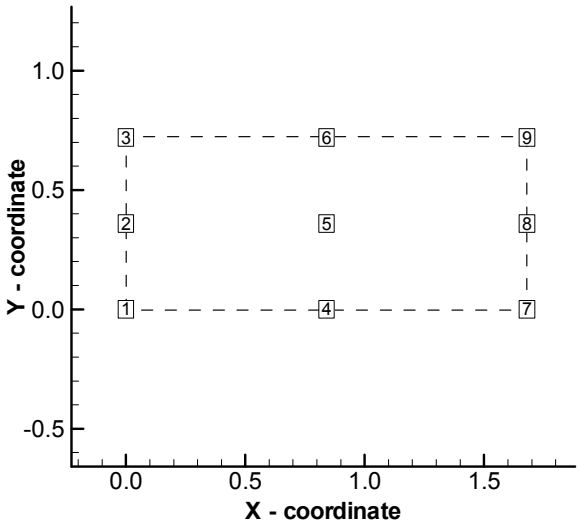

Figure 5. WIND FARM LAYOUT AS IN THE EXPERIMENT [13]

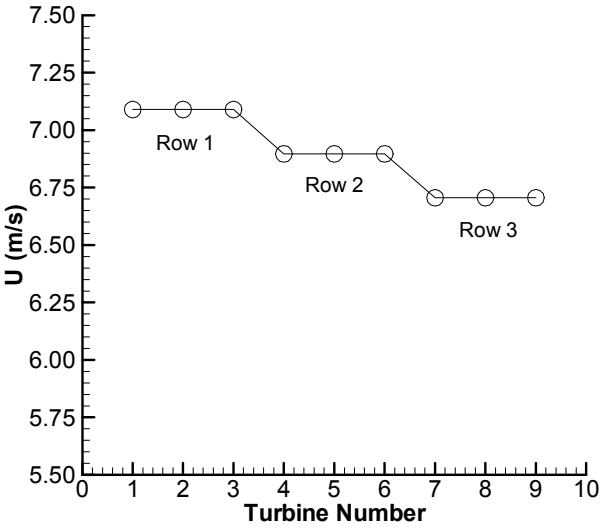

Figure 6. VELOCITY OF WIND (ESTIMATED) APPROACHING EACH TURBINE

In the experiment, extensive measurements (of different parameters) are made for Turbine-8 (last row, center turbine). The key parameters are calculated by the model and compared with those measured in the experiment [13] in Table 3.

Copyright © 2010 by ASME

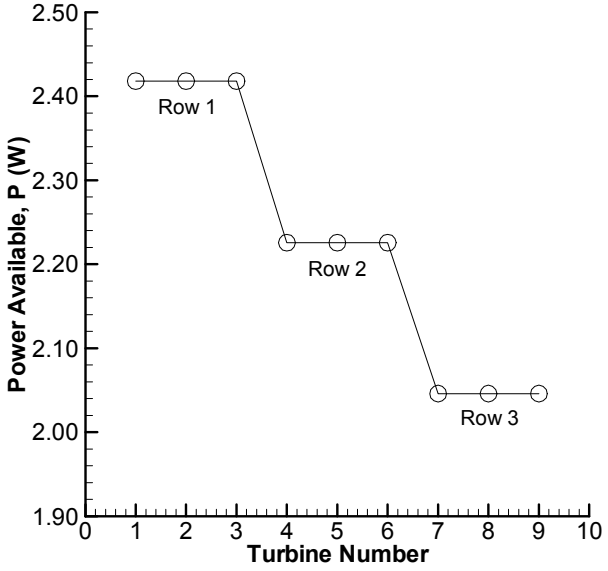

Figure 7a. POWER AVAILABLE (ESTIMATED) FOR EACH TURBINE

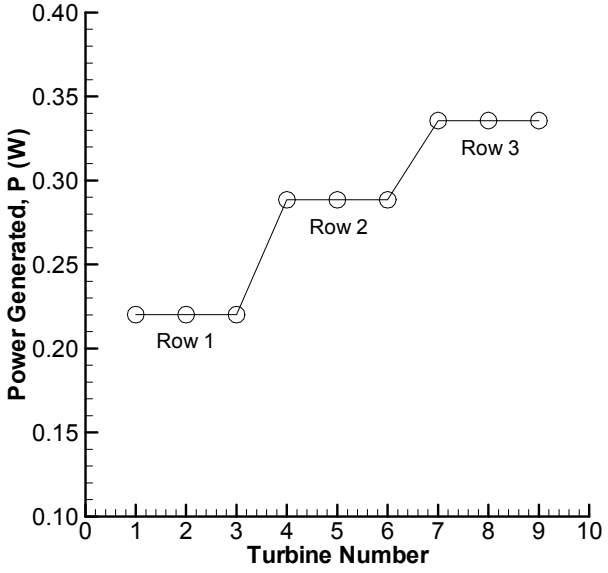

Figure 7b. POWER GENERATED (ESTIMATED) BY EACH TURBINE

Table 3. COMPARISON OF THE POWER GENERATION MODEL WITH THE EXPERIMENT (TURBINE-8)

Parameter	Wind Farm Model	Experiment
U in front of turbine	6.71 m/s	6.24 m/s
Power generated	0.336 W	0.34 W
C_p	0.16	0.21
a	0.085	0.087

It is seen from Fig. 6 and Table 3 that the model overestimates the velocity of the wind immediately in front of the last row center turbine (Turbine-8) by 7.53%. This difference can be attributed to the various assumptions made in the analytical wind farm model, such as uniform flow, no explicit consideration of turbulence, neglecting such factors as rotor inefficiencies and other wake model inaccuracies. However, the general trend of velocity deficit is appropriately captured by the model. Figures 7a and 7b show that, though the power available from wind for each turbine decreases downstream due to wake effects, the power generated by each turbine follows an opposite trend. The estimated power generation by Turbine-8, as seen from Fig. 7b and Table 3, is slightly less than that measured in the experiment. These observations are explained by the overall nature of the power curve (Fig. 4). The incoming wind (at 7.09 m/s) in this case is already above the optimal/rated wind speed (6.17 m/s); hence the power generated increases downstream (with decreasing wind velocity). The total power generated (refer Eq. (13)) by the farm and the corresponding normalized value are estimated to be 2.53 W and 0.73, respectively. The latter gives a measure of the farm efficiency.

CONSTRAINED PARTICLE SWARM OPTIMIZATION (PSO) ALGORITHM

PSO is one of the most well known stochastic optimization algorithms, initially coined by an Electrical Engineer (Russel Eberhart) and a Social Psychologist (James Kennedy) in 1995 [14]. Later, several improved variations of the algorithm have appeared in the literature and been used in popular commercial optimization packages. The PSO algorithm used in this project has been derived from the unconstrained version presented by Colaco et al. [27]. A general single objective constrained optimization problem is represented by Eq. (22).

$$\begin{aligned} &Min\ f(X) \\ &subject\ to \\ &g_j(X) \le 0, \quad \mathrm{j} = 1,2,...,p \\ &h_k(X) = 0, \quad \mathrm{k} = 1,2,...,q \end{aligned} \tag{22}$$

Here p and q are the number of inequality and equality constraints, and X is the vector of design variables. The basic steps of the algorithm followed in order to solve such a problem are summarized as

$$\begin{aligned} x_i^{t+1} &= x_i^t + v_i^{t+1} \\ v_i^{t+1} &= \alpha v_i^t + \beta_l r_1 \left(p_i - x_i^t \right) + \beta_g r_2 \left(p_g - x_i^t \right) \end{aligned} \tag{23}$$

where,
x_i^t is ith member of the population (swarm) at the tth iteration,
r_1 and r_2 are random numbers between 0 and 1,
p_i is the best candidate solution found for the ith member,
p_g is the best candidate solution for the entire population and
α, β_l and β_g are user defined constants in the range [0, 1].

Copyright © 2010 by ASME

The technique used to deal with constraints is based on the principle of constrained non-domination, introduced by Deb et al. [15]. In this technique, solution-*i* is said to dominate solution-*j* if,

- solution-*i* is feasible and solution-*j* is infeasible or,
- both solutions are infeasible and solution-*i* has a smaller constraint violation than solution-*j* or,
- both solutions are feasible and solution-*i* weakly dominates solution-*j*.

If none of the above conditions apply (possible only in the case of a multi-objective problem), then both of the solutions are considered non-dominated with respect to each other.

UWFLO GLOBAL OPTIMIZATION FRAMEWORK

The UWFLO setup has been applied to three different cases in order to investigate the extent of layout optimization for different wind farms as listed below.

1. Wind farms with identical turbines,
2. Wind farms with non-identical turbines and
3. Wind farms with identical turbines that can adapt to wind conditions (that better represent commercial wind turbines) and hence, usually operate close to the maximum of their performance curves.

UWFLO Case 1

In Case 1, the wind farm is comprised of a fixed number of identical wind turbines (with rotors diameters = D). The wind farm attributes (except for the layout) and the nature of the incoming wind are the same as given in Tables 1 and 2. Also, the turbines are assumed to be facing the incoming wind. The layout of the rectangular wind farm is optimized in order to achieve maximum power generation. The optimization problem is formulated as follows:

$$\begin{aligned} &Max\ f = \frac{P_{farm}(V)}{NP_0} \\ &subject\ to \\ &g_1(V) \le 0 \\ &V = \{X_1, X_2, ..., X_N, Y_1, Y_2, ..., Y_N\} \\ &0 \le X_i \le X_{farm} \\ &0 \le Y_i \le Y_{farm} \end{aligned} \tag{24}$$

P_0 is the maximum power that can be generated by an individual turbine which is calculated to be 0.385 W from the power curve shown in Fig. 4. The inequality constraint g_1 represent the minimum clearance required between any two adjacent turbines, and is given by the following equation

$$\begin{aligned} g_1(V) &= \sum_{i=1}^{N}\sum_{\substack{j=1 \\ j\neq i}}^{N} \max\left(\left(D_i + D_j + \Delta_{\min} - d_{ij}\right), 0\right) \\ d_{ij} &= \sqrt{\Delta x_{ij}^{\ 2} + \Delta y_{ij}^{\ 2}} \end{aligned} \tag{25}$$

Here, Δ_{min} is the minimum clearance required between the outer edge of the rotors of two adjacent turbines. The parameters X_{farm} and Y_{farm} in Eq. (24) represent the extent of the rectangular wind farm in X and Y directions. To ensure the placement of the wind turbines within the fixed size wind farm, the X_i and Y_i bounds are reformulated into an inequality constraint expressed by

$$\begin{aligned} &g_2(V) \le 0, \quad \text{where} \\ &g_2(V) = \frac{1}{2N}\left(\begin{aligned} &\frac{1}{X_{farm}}\sum_{i=1}^{N}\max\left(-X_i, X_i - X_{farm}, 0\right) \\ &+\frac{1}{Y_{farm}}\sum_{i=1}^{N}\max\left(-Y_i, Y_i - Y_{farm}, 0\right) \end{aligned}\right) \end{aligned} \tag{26}$$

UWFLO Case 1 Results

The objective of this study (Case 1) is to investigate the optimization of the placement of turbines in a wind farm which has the same attributes and is subjected to the same conditions as in the experiment [13]. The optimization is performed using the PSO algorithm, which is initiated with a population of random wind farm layouts. The user defined constants involved in PSO are summarized in Table 4.

Table 4. USER DEFINED CONSTANTS IN PSO

Constant	Value
α	0.5
β_g	1.4
β_l	1.4
Allowed number of function calls	15000

It is noteworthy that the optimum wind farm layout is not necessarily unique. There can be different optimal arrangements of turbines with nearly equal amount of total power output. This results in an optimization problem with multiple optima. To compensate for the performance fluctuations induced by random generators used in creating the initial population and other swarm operators, the algorithm was run five times each for each case. The outcomes of the one of the representative runs are shown each for case.

Figure 8 shows that the algorithm converges after approximately 3000 function evaluations during which the power generated by the farm increases by 15.54%. The power generated by the optimum farm layout (3.298 W) is 30.19% higher than that generated by the original farm layout in the experiment (Fig. 5).

Copyright © 2010 by ASME

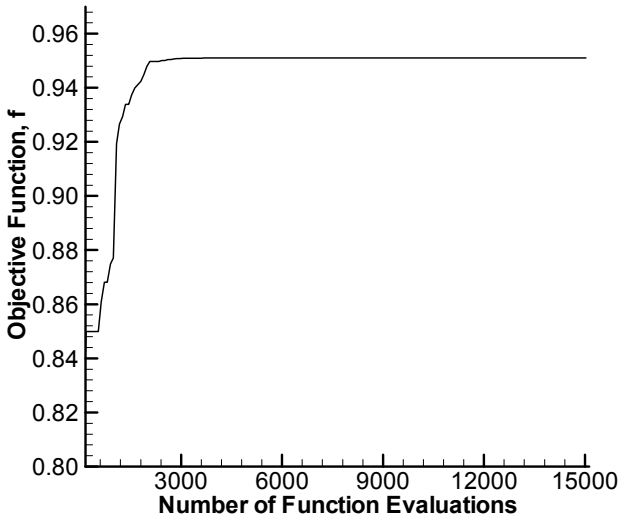

Figure 8. CONVERGENCE HISTORY OF PSO (CASE 1)

The increase in the power generated by the wind farm through unrestricted layout optimization is substantial. The optimum farm layout is shown in Fig. 9, and the power generated by each turbine of this wind farm is shown in Fig. 11. Figure 10 presents the wind velocity immediately in front of each turbine. The latter two figures are plotted with respect to the turbine number since the turbine numbers are equivalent to the rank of the turbines that represents the order in which the turbines encounter the incoming wind. Thereby, a discrete manifestation of the nature variation of P and U in the downstream direction is provided.

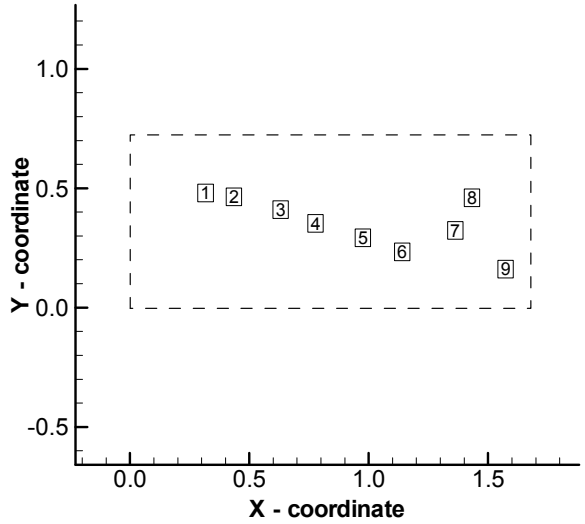

Figure 9. OPTIMIZED WIND FARM LAYOUT (CASE 1)

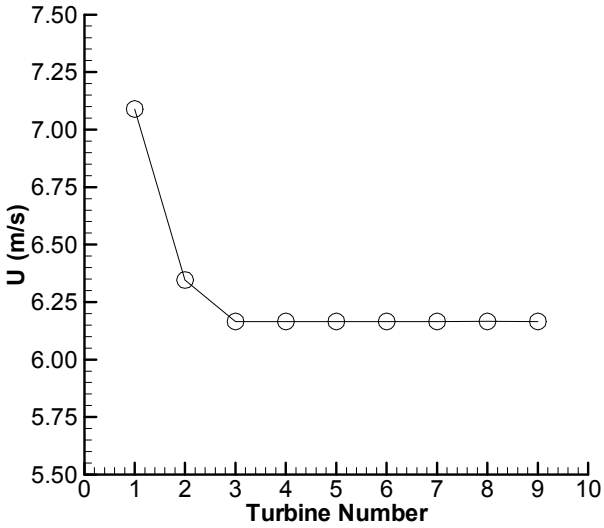

Figure 10. VELOCITY OF WIND APPROACHING EACH TURBINE (U) IN THE OPTIMIZED WIND FARM (CASE 1)

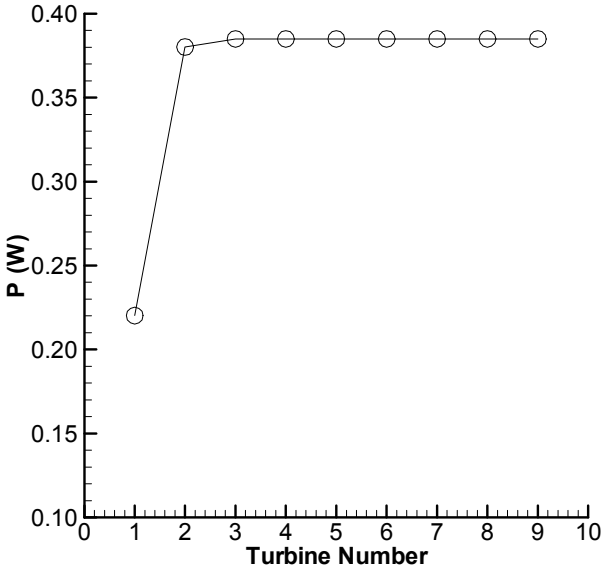

Figure 11. POWER GENERATED BY EACH TURBINE (P) IN THE OPTIMIZED WIND FARM (CASE 1)

It is readily observed from Figs. 10 and 11 that the optimization procedure endeavored to arrange the turbines in a manner such that most of them operate near the maximum power generation point of the power curve (i.e. U = 6.17 m/s as seen from Fig. 4). This phenomenon explains the deliberate positioning of some turbines in the wakes of others, upwind, in order to have an approaching wind velocity as close as possible to the operating ideal. Only Turbine-1 does not have the liberty to choose an appropriate location since it always has to face the incoming wind, and hence generates less power

Copyright © 2010 by ASME

than the other turbines located downstream (since incoming wind speed is greater than rated speed of 6.17 m/s). Nevertheless, in the case of a commercial wind farm the scenario may be quite different. This is because real life wind turbines are designed to orient themselves (such as by changing the pitch and yaw angle) in order to extract maximum power from the wind while operating within other constraints such as structural limitations. Hence the power curve and the performance characteristics of real life wind turbines (details available in the Wind Energy Handbook [1]) are more complex than the simple scaled down model turbines used in the experiment [13]. However, the performance characteristics are simply inputs to the UWFLO model. The optimization results demonstrate that the UWFLO model is expected to produce reliable results for real life wind farms as long as the correct performance curves are provided.

UWFLO Case 2

This case is similar to Case 1, except that the wind turbines are allowed to have different rotor diameters. During optimization, the rotor diameter of each turbine is treated as a design variable. Hence there are a total of *3N* design variables in Case 2 as opposed to *2N* variables in Case 1. The cost of a wind farm as a function of the individual turbine diameters is included as an additional constraint ($g_3 = Cost$). In order to maximize the power generated by the wind farm, the optimization problem is formulated as follows.

$$
\begin{aligned}
&Max\ f = \frac{P_{farm}(V)}{NP_0} \\
&subject\ to \\
&g_1(V) \le 0 \\
&g_2(V) \le 0 \\
&g_3(V) \le 0 \qquad (27) \\
&V = \{X_1, X_2, ..., X_N, Y_1, Y_2, ..., Y_N, D_1, D_2, ..., D_N\} \\
&0 \le X_i \le X_{farm} \\
&0 \le Y_i \le Y_{farm} \\
&D_{\min} \le D_i \le D_{\max}
\end{aligned}
$$

UWFLO Case 2 Results

The objective of this study (Case 2) is to explore the effect of having non-identical wind turbines (different rotor diameters) on the total power generation from the wind farm. The above demands simultaneous optimization of the location and the rotor diameter of each turbine placed in the wind farm. The rotor diameter based cost of the farm (Eq. (18) and (19)) is implemented as an additional constraint $g_3(V)$. This constraint ensures that any feasible solution represents a wind farm that demands a net investment equal to or less than that for a wind farm with identical wind turbines. The mean rotor diameter and the deviation in diameter, calculated from the data used to estimate the cost function, are 75m and ±25m, respectively. This data, when scaled down to the dimensions of the model turbines used in the experiments (D = 0.12m), results in a deviation of ±0.04m. Thus, the feasible range of rotor diameter was specified as 0.08 – 0.16 m/s. The wind farm simulated in Case 2 has the same attributes (except the rotor diameters) and is subjected to the same conditions as given in Tables 1 and 2, respectively. The PSO algorithm is run with the constants given in Table 4, except for a specification of 25000 function evaluations. This increase in the allowed number of function evaluations can be attributed to the significant increase in the dimensionality of the problem (due to 9 additional design variables).

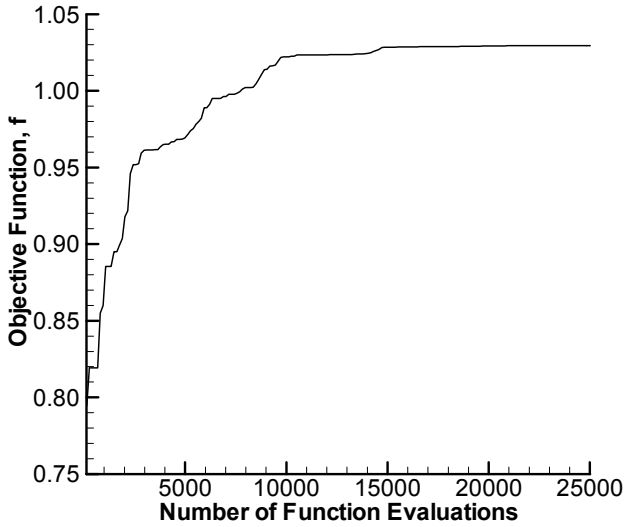

Figure 12. CONVERGENCE HISTORY OF PSO (CASE 2)

Figure 12 shows that the algorithm converges after approximately 15,000 function evaluations during which the power generated by the farm increases by 28.75%. The power generated by the optimum farm layout (3.569 W) is 41.11% higher than that generated by the original farm layout in the experiment (Fig. 5). It should be noted that the maximum possible power generation from a single turbine in this case is not restricted by the power curve shown in Fig. 4, since the rotor diameters can be higher than the rotor diameters of the model turbines used in the experiment. Consequently, the normalized value of the total power generated is not an appropriate manifestation of the farm efficiency in Case 2 and can reach values higher than unity as shown in Fig. 12. The optimum farm layout is shown in Fig. 13, and the wind velocity immediately in front of each turbine is shown in Fig. 14. Figures 15 and 16 present the power generated by each

Copyright © 2010 by ASME

turbine and the rotor diameter of each turbine in the optimum wind farm, respectively.

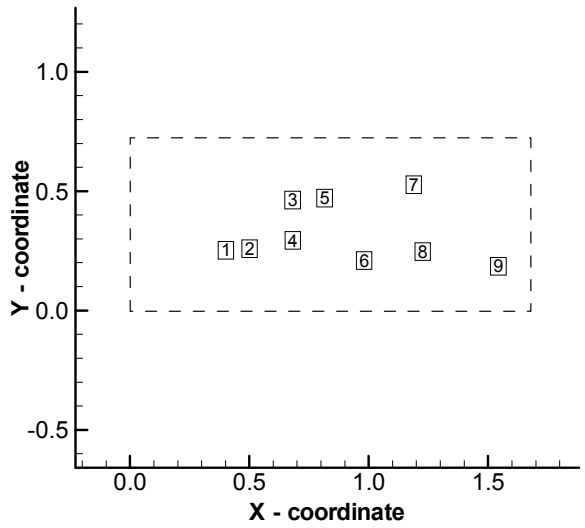

Figure 13. OPTIMIZED WIND FARM LAYOUT (CASE 2)

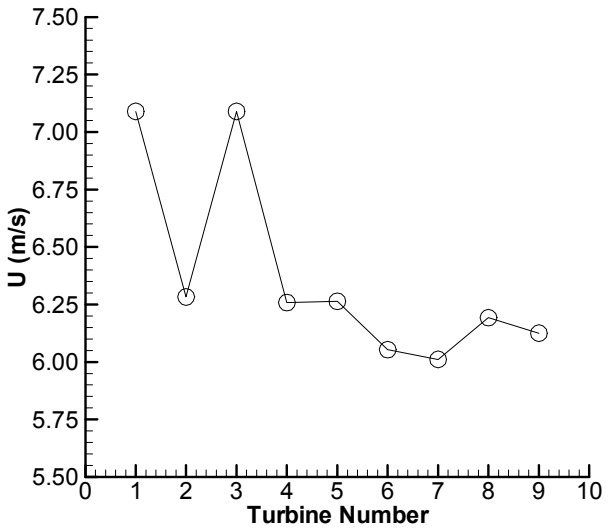

Figure 14. VELOCITY OF WIND APPROACHING EACH TURBINE IN THE OPTIMIZED WIND FARM (CASE 2)

The specific rotor diameters for each turbine (Fig. 16) and the corresponding farm layout (Fig. 13), resulting from the optimization process, produces an interesting distribution of the approaching wind velocity and the power generated in the case of each turbine. An intuitive investigation of the optimum combination of turbines with different rotor diameters and the optimum placement of the same within the wind farm is a task of considerable difficulty. The most important observation from the results of Case 2 is the remarkable increase in the total power generated by the wind farm, accomplished using non-identical turbines.

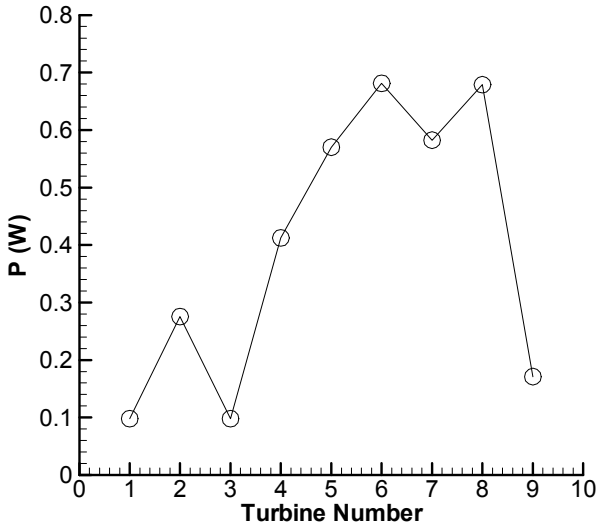

Figure 15. POWER GENERATED BY EACH TURBINE IN THE OPTIMIZED WIND FARM (CASE 2)

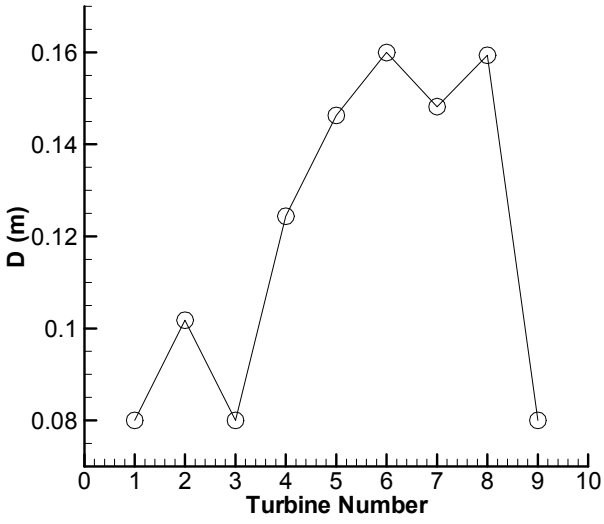

Figure 16. ROTOR DIAMETER OF EACH TURBINE IN THE OPTIMIZED WIND FARM (CASE 2)

The rotor diameter has been considered as a continuous variable in this study, whereas commercial wind turbines present a discrete variation of the same. Also, non-identical wind turbines might have different performance characteristics. In this study, such data was not available and hence the same performance curves (as in Fig. 3) were used for all turbines. In the case of a commercial wind farm, the total cost is a complex function of various physical and

Copyright © 2010 by ASME

economic factors. Hence, more realistic results can be obtained if the following are taken into account:

1. Treatment of turbine rotor diameters as discrete variables
2. Use of appropriate performance characteristics
3. Application of a comprehensive cost model

UWFLO Case 3

Case 3 presents the same optimization problem as in Case 1 with an exception. Namely, constant values of C_p and a, equal to their individual maximums (0.3125 and 0.095, respectively) are used instead of that given by the performance curves shown in Fig. 3. Consequently, the power generated by each turbine is directly proportional to the cube of the approaching wind velocity; all other parameters (Eq. (11)) remain the same for the wind farm. In this case the power generated by the wind farm is normalized using P_0' (Eq. (28)) instead of P_0, so that the objective function represents the farm efficiency more appropriately.

$$P_0' = C_{p,\max}\left(\frac{1}{2}\rho\pi\frac{D^2}{4}U_0^{\,3}\right) \tag{28}$$

UWFLO Case 3 Results

Case 3 demonstrates the suitability of UWFLO for commercial wind farms. The primary difference between commercial wind turbines and those designed for the experiment is the absence of pitch variability that is used to adapt to wind conditions. This design of scaled turbine models is an acceptable approximation in experiments if the inflow velocity is maintained constant. However such design would be significantly inefficient for a commercial wind farm. In commercial wind farms, the total power generated closely follows the trend of the total effective power available from the wind (for each turbine). The latter is highly sensitive to the wake effects. As a result, it is important to investigate the outcomes of layout optimization with the objective of reducing energy deficits due to wake effects. The parameter, P_0', as expressed in Eq. (28) is calculated to be 6.80 W.

It is seen from Fig. 17 that the optimization process converges after approximately 7500 function evaluations, yielding an increase of 5.62% in the total power generated by the wind farm; this power is 7.97% higher than that generated by the original farm layout in the experiment. The latter is also calculated using constant C_p and a in this case. The optimum farm layout, the velocity of the wind approaching each turbine and the power generated by each turbine are shown in Fig. 18, 19 and 20, respectively.

The optimized layout as seen from Fig. 18 displays a more spread out arrangement of wind turbines when compared to the layout obtained in Case 1. Turbines 1, 2, 3, 4 and 5 face the incoming wind directly (Fig. 19), thereby, producing the maximum possible power generation (as depicted in Fig. 20). Turbines 6, 7, 8 and 9 are affected by the wakes of turbines upstream to them, respectively. Hence, Turbine 6, 7, 8 and 9 experience lower approaching wind velocities (Fig. 19), thereby, producing slightly less power than the turbines upstream (Fig. 20). However, it is evident from the layout shown in Fig. 18 that these turbines (turbines 6 – 9) are located significantly far downstream to minimize the net effect of the wakes produced by the preceding turbines (turbines 1 – 5). The significantly different nature of results obtained in Case 1 and Case 3 demonstrates that the optimum layout of a wind farm is very sensitive to the performance characteristics of the individual turbines.

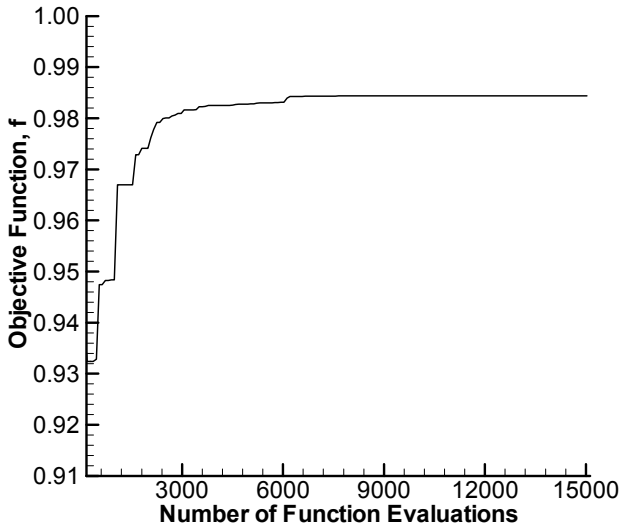

Figure 17. CONVERGENCE HISTORY OF PSO (CASE 3)

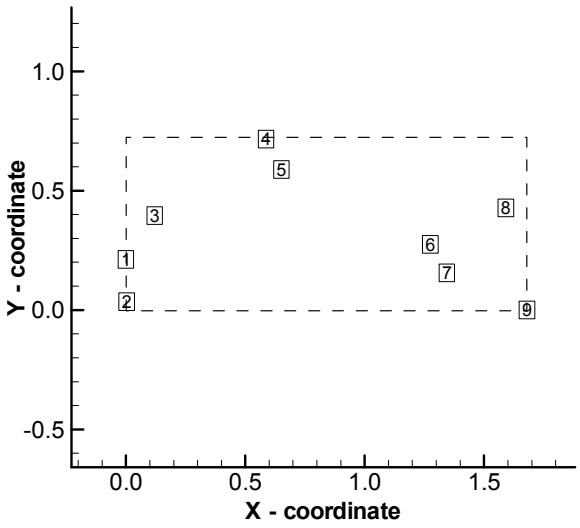

Figure 18. OPTIMIZED WIND FARM LAYOUT (CASE 3)

Copyright © 2010 by ASME

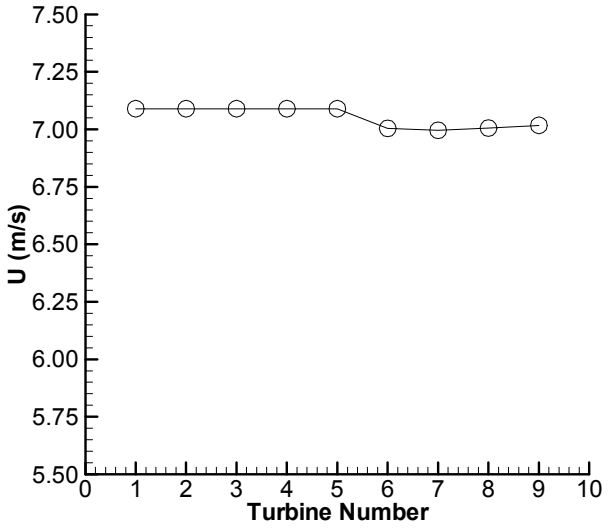

Figure 19. VELOCITY OF WIND APPROACHING EACH TURBINE IN THE OPTIMIZED WIND FARM (CASE 3)

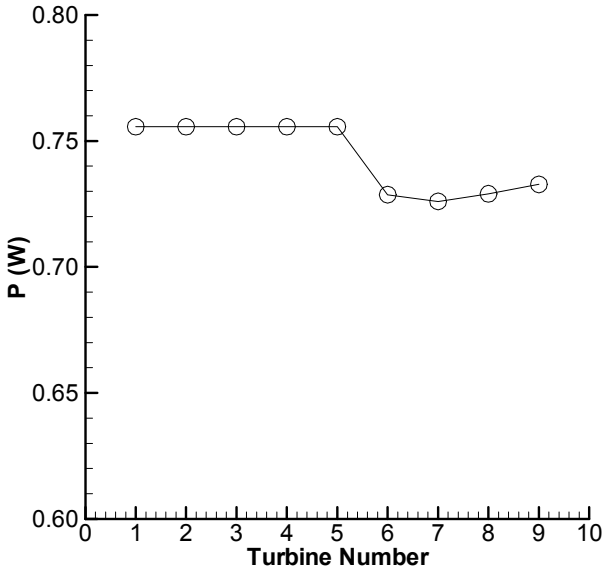

Figure 20. POWER GENERATED BY EACH TURBINE IN THE OPTIMIZED WIND FARM (CASE 3)

Such layout optimization (as in UWFLO) would be more pertinent to the commercial wind farm scenario, if an appropriate distribution of incoming wind velocities and directions and the exact performance characteristics of the wind turbines were used.

It was stated earlier that the optimum layout of wind farms, both with identical and non-identical turbines, is not necessarily unique; for example, a mirror image of the optimized farm layout would yield the same power generation. The five separate PSO runs for each case produced different optimum layouts of the wind farm, which substantiates the above statement. However, the variance in the total power generated is small across the five optimizations. Table 5 summarizes the maximum improvement in the power generated obtained by UWFLO, for the three different cases. The improvement, in the total power generated by the wind farm through layout optimization, has been calculated relative to the power generated (estimated) by the 3x3 experimental wind farm (Fig. 5).

Table 5. IMPROVEMENT IN POWER GENERATED BY THE WIND FARM THROUGH UWFLO (FIVE RUNS)

Case	Increase in Total Power (W)	Increase in Farm Efficiency	Percentage Increase *
1	0.76	0.22	30.19%
2	1.09	0.31	43.03%
3**	0.49	0.07	7.97%

* Percentage calculated with respect to power generated by experimental wind farm.

** Improvements calculated with respect to power generated by the experimental wind farm assuming constant C_p and a.

CONCLUSION

The UWFLO model presents a layout optimization technique that does not make limiting assumptions regarding the arrangement of turbines in a wind farm. It is successfully validated against data measured in a wind tunnel experiment of a scaled down wind farm [13]. The slight differences, between the values of the parameters estimated by the model and corresponding data from the experiment, can be ascribed to the standard assumptions made in the analytical modeling of the wake velocity deficits. Layout optimization is performed on a wind farm that is subjected to the same conditions, as in the experiment. This wind farm is comprised of turbines with the same performance characteristics as the model turbines in the experiment. A significant increase (30% compared to the experimental farm) in the total wind farm power generation is realized as the layout orients itself such that most of the turbines operate close to the maximum point given by the power curve.

A second case was studied, where the turbines in the wind farm were allowed to have different rotor diameters. A cost model, based on the rotor diameter of constituent wind turbines, was implemented to present an economically realistic scenario. A significantly higher improvement in the total power generated (43% compared to the experimental farm) was observed in this case, which accentuates the potential benefits of using of non-identical turbines in a wind farm. However, further research with a discrete distribution of available rotor diameters, pertinent performance characteristics and a more realistic cost model, would give a better insight in this direction. It was also observed that the farm layout is very sensitive to the performance characteristics of the wind turbines. Hence, a higher amount of available

Copyright © 2010 by ASME

power would not necessarily lead to higher power generation. Nevertheless, commercial wind turbines are more adaptive to wind conditions and have performance characteristics distinct from those of the model turbines used in the experiment. Therefore, optimization of the layout of a commercial wind farm would tend to maximize the sum of powers available for each constituent turbine. This phenomenon, however, does not limit the applicability of the UWFLO model to an actual wind farm. This model is expected to provide reliable results, as long as it is provided with pertinent inputs specific to the prevailing conditions and the turbines used in the wind farm.

The performance of the UWFLO model has been tested under conditions of unidirectional constant wind velocity. In the case of an actual farm, wind conditions are variable, even within a small time frame. Further research needs to be done by subjecting the wind farm model to a distribution of incoming wind velocities and other conditions similar to an existing commercial wind farm. Such a study would provide a better understanding of the sensitivity of the total power generation to the various factors involved in wind farm planning.

ACKNOWLEDGMENTS

Support from the National Science Foundation (Awards CMMI-053330 and CMII-0946765) is gratefully acknowledged.

REFERENCES

[1] Burton, T., David, S., Jenkins, N., and Ervin, B. Wind Energy Handbook. John Wiley & Sons, 2001.

[2] World Wind Energy Report 2008. Bonn, Germany, February 2009.

[3] Sorensen, P. and Nielsen, T. Recalibrating Wind Turbine Wake Model Parameters - Validating the Wake Model Performance for Large Offshore Wind Farms. In European Wind Energy Conference and Exhibition (Athens, Greece February 2006).

[4] Beyer, H. G., Lange, B., and Waldl, H. P. Modelling Tools for Wind Farm Upgrading. In Proceedings of European Union Wind Energy Conference, AIAA (Goborg, Sweden May, 1996).

[5] Elkinton, C., Manwell, J., and McGowan, J. Offshore Wind Farm Layout Optimization (OWFLO) Project: Priliminary Results. In 44th AIAA Aerospace Sciences Meeting and Exhibit, AIAA (Reno, Nevada January, 2006).

[6] Katic, I., Hojstrup, J., and Jensen, N. O. A Simple Model for Cluster Efficiency. In Proceedings of European Wind Energy Conference and Exhibition (Rome, Italy 1986).

[7] Jensen, N. O. A Note on Wind Turbine Interaction. Riso-M-2411, Roskilde, Denmark, 1983.

[8] Ainslie, J.F. Development of an Eddy Viscosity Model for Wind Turbine Wakes. In Proceedings of the 7th BWEA Wind Energy Conference (Oxford, UK 1985), 61-66.

[9] Mosetti, G., Poloni, C., and Diviacco, B. Optimization of Wind Turbine Positioning in Large Wind Farms by Means of a Genetic Algorithm. Journal of Wind Engineering and Industrial Aerodynamics, 54, 1 (January 1994), 105-116.

[10] Grady, S. A., Hussaini, M. Y., and Abdullah, M. M. Placement of Wind Turbines Using Genetic Algorithms. Renewable Energy, 30, 2 (February 2005).

[11] Sisbot, S., Turgut, O., Tunc, M., and Camdali, U. Optimal positioning of Wind Turbines on Gökçeada Using Multi-objective Genetic Algorithm. Wind Energy (2009).

[12] Frandsen, S., Barthelmie, R., Pryor, S, Rathmann, O, Larsen, S, Hojstrup, J, and Thogersen, M. Analytical Modeling of Wind Speed Deficit in Large Offshore Wind Farms. Wind energy, 9, 1-2 (2006), 39-53.

[13] Cal, R. B., Lebron, J., Kang, H.S., Meneveau, C., and Castillo, L., "Experimental study of the horizontally averaged flow structure in a model wind-turbine array boundary layer", submitted to Journal of Renewable and Sustainable Energy, August 2009.

[14] Kennedy, J. and Eberhart, R. C. Particle Swarm Optimization. In Proceedings of the 1995 IEEE International Conference on Neural Networks (1995), 1942-1948.

[15] Deb, K., Pratap, A., Agarwal, S., and Meyarivan, T. A Fast and Elitist Multi-objective Genetic Algorithm: NSGA-II. IEEE Transactions on Evolutionary Computation, 6, 2 (April 2002), 182-197.

[16] Chowdhury, S. and Dulikravich, G. S. Improvements to Single-Objective Constrained Predator–Prey Evolutionary Optimization Algorithm. Structural and Multidisciplinary Optimization (September 2009 (Online)).

[17] Betz, A. Introduction to the Theory of flow Machines (Translated by Randall, D. J.). Pergamon Press, 1966.

[18] Lanchester, F. W. Contribution to the theory of propulsion and the screw propeller. Transactions of the Institution of Naval Architects, 57 (1915), 98-116.

[19] Frandsen, S. On the Wind Speed Reduction in the Center of a Large Cluster of Wind Turbines. Journal of Wind Engineering and Industrial Aerodynamics, 39 (1992), 251-265.

[20] Kiranoudis, C., Voros, N., and Maroulis, Z., 2001, "Shortcut design of wind farms". Energy Policy, 29, pp. 567–578.

[21] Kaldellis, J. K., and Gavras, T. J., 2000, "The economic viability of commercial wind plants in Greece a complete sensitivity analysis". Energy Policy, 28, pp. 509–517.

[22] Herman, S., 2002, Probabilistic cost model for analysis of offshore wind energy costs and potential. Technical Report ECN-I–02-007, Energy Research Centre of the Netherlands, May.

[23] National Renewable Energy Laboratory, 2009, Jobs and Economic Development Impact (JEDI) Model. Golden, Colorado, US, October.

Copyright © 2010 by ASME

[24] Cockerill, T. T., 1997, Methods assisting the design of OWECS part a: Concept analysis, cost modeling and economic optimization. Technical Report JOR3-CT95-0087, Renewable Energy Centre, University of Sunderland.
[25] Kang, H. S. and Meneveau, C., 2009, "Direct mechanical torque sensor for model wind turbines", submitted to Wind Energy, December.
[26] Lebron, J., Castillo, Cal, R. B., Kang, H. S., and Meneveau, C., 2010, "Interaction Between a Wind Turbine Array and a Turbulent Boundary Layer," Proceeding 49th AIAA Aerospace Sciences Meeting including the New Horizons Forum and Aerospace Exposition, January 4-9.
[27] Colaco, M. J., Orlande, H. R. B., and Dulikravich, G. S. Inverse and Optimization Problems in Heat Transfer. Journal of the Brazilian Society of Mechanical Science and Engineering, 28, 1 (2006).

Copyright © 2010 by ASME